Combined excitation-emission spectroscopy of Er^{3+} ions in stoichiometric $LiNbO_3$: The site selectivity of direct and up conversion excitation processes

V. Dierolf and M. Koerdt
Fachbereich Physik, Universität Paderborn, Warburger Strasse 100, D33098 Paderborn, Germany
(Received 7 June 1999)

We studied the optical transitions of Er^{3+} ions in $LiNbO_3$ for samples with stoichiometric composition that were produced from congruent ones by the vapor transport equilibration technique. Using combined excitation-emission as well as absorption, emission, and Raman spectroscopy with high resolution, we found and spectrally characterized a large number (>11) of different Er^{3+} sites. Comparing stoichiometric and congruent samples we found equivalent sites, however, with an altered distribution of their abundances. For the microscopic origin of the sites we propose that for the main sites the Er^{3+} is located on or close to a Li^+ lattice site with differing arrangements of the required local charge compensation. On the basis of these results we investigated in detail the upconversion process that occurs under 980-nm excitation and found several mechanisms including direct and phonon-assisted excited state absorption and energy transfer, which are all strongly dependent on site and on the excitation energy.

I. INTRODUCTION

The combination of excellent electro-optical, acousto-optical, and nonlinear optical properties and the possibility to produce low-loss optical waveguides makes lithium niobate ($LiNbO_3$) an attractive material for applications in integrated optics and actually has been used successfully for various optical components (e.g., modulators, wavelength filters). Moreover, the incorporation of Er^{3+} ions allows us to realize active devices such as optical amplifiers and lasers, which have been demonstrated for the important 1.5-μm region.[1] Besides this emission transition from the $^4I_{13/2}$ to the $^4I_{15/2}$ state, which can be efficiently pumped using semiconductor lasers at 1.48 μm and 980 nm, the Er^{3+} ion offers a variety of other transitions and excitation possibilities (see Fig. 1), for which laser operation was achieved in various materials [e.g., $LiYF_4$,[2–4] yttrium aluminum garnet[5] (YAG), fluoride glass fibers[6]]. Of particular interest are upconversion lasers at around 550 nm, which can be excited via a two-step process with 980-nm laser diodes and ir lasers at around 3 μm for which upconversion and cross relaxation play a major role in the population dynamics.[7] Driven by these existing and potential applications, several studies of the structural and optical properties of the Er^{3+} ion in $LiNbO_3$ exist. With respect to the Er^{3+} incorporation into $LiNbO_3$, it was found by several techniques, i.e., x-ray standing waves (XSW),[8,9] Rutherford backscattering,[10] extended x-ray absorption fine structure[11] (EXAFS), and ion beam channeling,[12] that the Er^{3+} occupies a Li^+ site in the crystal lattice. On the other hand, several optical and magnetic resonance spectroscopy studies revealed that not just one but several slightly different types of center configurations or lattice environments exist.[13–19] The number and origin of these optically different Er^{3+} ions, which we will refer to in the following often as ''sites,'' as well as their dependence on sample preparation are unclear and still under debate.

Most studies performed so far are limited to the congruent $LiNbO_3$ composition (Li/Nb=0.92), which can be grown most easily. Much less work has been performed, so far, for stoichiometric (Li/Nb=1) samples. This $LiNbO_3$ crystal type exhibit less ''optical damage'' caused by the photorefractive effect, a property that may prove to be essential to achieve laser operation in the visible region. In this work we concentrated on the stoichiometric samples and explored—besides the general optical properties of the Er^{3+} ion within this well-ordered sample composition—the following questions:

(1) How many discretely different Er^{3+} environments exist?

(2) What are the differences between congruent and stoichiometric samples in respect to the nature of the Er^{3+} sites and their distribution?

(3) How strongly do the different Er^{3+} sites participate in

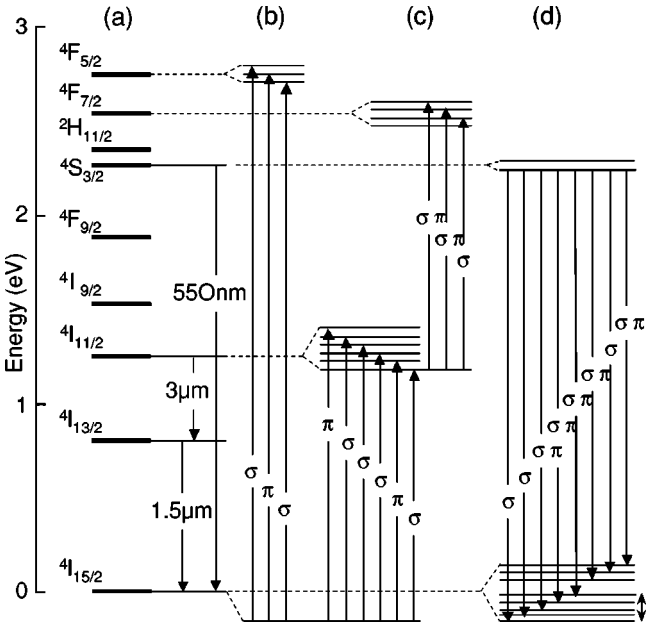

FIG. 1. Schematic energy level diagrams of Er^{3+} in $LiNbO_3$. On the right side, the energy levels and transitions studied in this work are shown in more detail. The expected polarization of the transitions for C_3 symmetry is indicated.

 ©2000 The American Physical Society

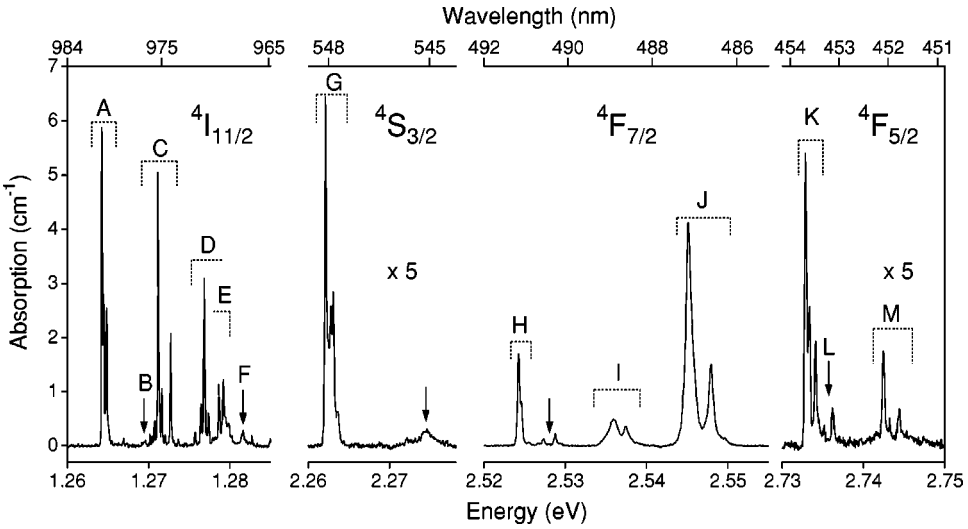

FIG. 2. Absorption spectra observed in α polarization for those final states $^4F_{5/2}$, $^4F_{7/2}$, $^4S_{3/2}$, and $^4I_{11/2}$ most relevant for this study. The allowed σ-type transitions are labeled by letters $(A,\ldots,M)$. The π transitions are marked additionally by arrows.

the upconversion processes and what are the underlying mechanisms?

Following the description of the sample preparation and experimental techniques in Sec. II and the presentation of the experimental results in Sec. III, we will discuss these questions in Sec. IV.

II. SAMPLE PREPARATION AND EXPERIMENTAL TECHNIQUES

The $LiNbO_3$ samples used in this work,[20] which are identical to those used in earlier works[14,18] were grown from the congruent melt to which Er^{3+} dopant was added (0.19 mol %). The achieved Er^{3+} concentration of $\approx 3\times 10^{19}$ cm^{-3} in the crystal was determined by absorption measurements and is intentionally very close to the average concentration achieved in typical diffusion doped Ti:Er:$LiNbO_3$ waveguides.[13] The congruent samples were converted to the approximately stoichiometric composition by the vapor transport equilibration (VTE) method.[21–23] For comparison identical pieces cut out of the same wafer were kept as reference. The Li/Nb ratio x was determined by the phase-matching temperature for second-harmonic generation of 1.064-μm light to be 0.998. This almost perfect stoichiometry was confirmed in Raman measurements by the width of the phonon mode (E) at 19 meV (Ref. 24) and by the spectral shape of the ir absorption from unintentionally present OH^- impurities.[25,26] The sample pieces were oriented by x-ray diffraction and cut so that the crystallographic c axis is perpendicular to the main surface (''z cut''). This allowed us to measure the absorption, Raman, and emission spectra for the signal light propagating along the c axis (α polarization). For the respective laser excitation a light polarization parallel (π) or perpendicular (σ) to the optical axis could be used. For high spectral selectivity we employed the method of combined excitation-emission spectroscopy (CEES) by which a very high selectivity can be achieved. In this technique, used already in a similar way by Gill *et al.*,[16] a large number of emission spectra ($\geqslant 200$) is recorded at a dense sequence of excitation energies using a 0.85-m double monochromator (Spex 1402) and an optical multichannel analyzer (OMA, SI IRY700). The samples were excited by cw dye ($\approx$450 nm) and Ti:sapphire lasers ($\approx$980 nm) with the wavelength controlled by a wavemeter (Burleigh WA2500). The spectral resolution for both excitation and emission photon energy was better than 0.1 meV. The whole setup was computer controlled to minimize measuring time. The resulting two-dimensional (2D) data set of emission intensities as a function of emission and excitation wavelength $I(\lambda_{em},\lambda_{exc})$ or energy $I(E_{em},E_{exc})$ is best visualized using a contour plot in which lines of equal emission intensities are drawn. In such a representation, a single emission line excited in a single absorption appears—similar to a geographic map—as a mountain. In this data representation the spectral responses of Er^{3+} ions that are situated in different crystal environments and have altered transition energies can easily be distinguished. The measurements, which will be presented in the following, were performed at low temperature ($T\approx 5$ K) in a He-flow cryostat on stoichiometric samples, unless stated otherwise.

III. EXPERIMENTAL RESULT

A. Regular absorption, emission, and excitation spectroscopy

In Fig. 2 the absorption spectra in several spectral regions are shown for the stoichiometric $LiNbO_3$ sample recorded at $T=5$ K in α polarization. In all depicted regions the transitions are electric-dipole forced and hence the results for α and σ polarization are identical. For the C_3 site symmetry all (except Kramer's) degeneracy of the states is removed, resulting in $J+\frac{1}{2}$ Stark split sublevels. In our measurements all $\sigma(\alpha)$-polarized transitions (see also Fig. 1) originating from the lowest sublevel of the $^4I_{15/2}$ state are observed and are labeled for further reference by letters. $(A,\ldots M)$ Even some of the π transitions, which are forbidden in C_3 symmetry, can be seen and are pointed out as arrows in Fig. 2. In general, the lines are very narrow with full widths at half maximum (FWHM) down to 0.1 meV much less than those for congruent samples. For that reason it is possible to clearly resolve within the individual transitions a substructure

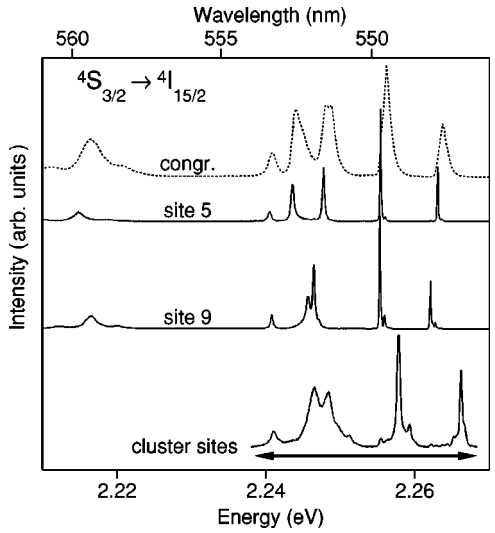

FIG. 3. $^4S_{3/2} \rightarrow {}^4I_{15/2}$ emission spectrum obtained under direct excitation into the $^4F_{5/2}$ for 3 slightly different excitation energies showing spectra for site 5, site 9, and for cluster sites. For comparison a spectrum in a congruent sample is shown by dotted lines. For identification and labeling of sites see Fig. 6 and its discussion in the text. The spectral range depicted in Fig. 5 is indicated by an arrow.

clearly showing that more than one Er^{3+} site exists. Several transitions (e.g., I,J) are notably much broader. This phenomenon appears whenever the distance within the Stark sublevels coincides with the energy of a phonon, causing a fast relaxation of the level[27] leading to a lifetime-determined (homogeneous) spectral width.

By excitation of the ions into the $^4F_{5/2}$ state [Fig. 1(b)] and subsequent fast relaxation the characteristic green luminescence [Fig. 1(d)] is obtained and shown in Fig. 3. Again, it is obvious that the emission lines are much narrower for the stoichiometric samples compared to the congruent sample, which is shown for comparison. Moreover, the effect of line narrowing is much more pronounced than stated by Gill *et al.*,[19] giving further evidence for the excellent optical quality and highly stoichiometric composition of our samples. Under slight variation of the excitation energy the spectral positions of the emission lines are strongly altered. As an example three such spectra are shown, representing different sites that we will identify in more detail below. In all spectra a clear substructure can be seen, although much less complicated than that in absorption due to the higher selectivity.

In Fig. 4 the excitation spectrum for the integrated green luminescence is shown. The spectrum obtained under σ-polarized excitation resembles closely the absorption spectrum (K,L,M in Fig. 2), but more details can be resolved due to the better signal-to-noise ratio. In accordance to the selection rules expected for C_3 symmetry the spectrum under π excitation reveals the in the α-absorption spectrum missing or weak transitions. Further details of this polarization dependence can be obtained from the degree of polarization (DP) calculated from the emission intensities I_σ and I_π under σ and π excitation as follows:

$$\mathrm{DP} = \frac{I_\sigma - I_\pi}{I_\sigma + I_\pi}. \tag{1}$$

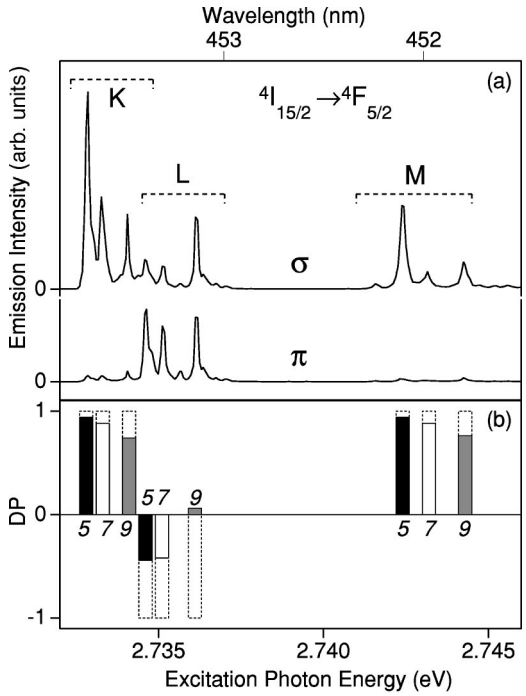

FIG. 4. (a) Excitation spectra for σ- and π-polarization probed broadband around 550 nm. (b) Degree of polarization shown as bars at the spectral positions of peaks in (a). The gray scale of the bars indicates the assignment to different sites. The dashed bars show the behavior expected for C_3 symmetry. For identification and labeling of sites see Fig. 6 and its discussion in the text.

The result is shown in Fig. 4(b) with bars for several peak positions of the excitation spectrum. The different shades of gray reflect the assignment (performed in the following sections) of the peaks to different Er^{3+} types. For sites 5 and 7 one finds good agreement with the behavior expected for a perfect C_3 symmetry (shown as a dotted line), especially in the σ-type transition. The less perfect degree of polarization may at least partially be due to small misalignments of light polarization and/or the samples. Despite this experimental uncertainty, it is clearly seen that for site 9 the polarization behavior is drastically different. In the region of the expected π excitation the transition is almost polarization independent and even the other transitions are much less polarized than expected.

B. Combined excitation-emission spectroscopy (CEES)

The results presented so far give already a lot of evidence that several different Er^{3+} sites are present even in the stoichiometric sample. Although in principle it would be possible to distinguish them by traditional emission and excitation spectroscopy, the number of sites and their spectral lines that partially overlap makes the application of the more systematic approach of CEES advisable and rewarding.

1. Direct excitation

In Fig. 5 the contour plot for a large number of emission spectra in the excitation range of the three transitions $^4I_{15/2} \rightarrow {}^4F_{5/2}$ is shown. Out of the eight emission lines we select the five (indicated in Fig. 3) that have a small enough spectral width to ascertain high selectivity and moreover fit well

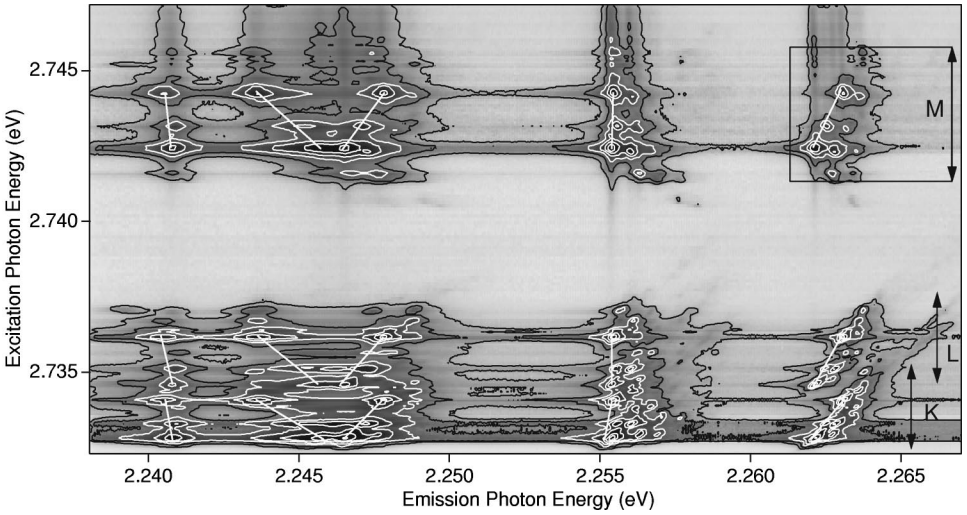

FIG. 5. CEES survey spectra of the green $^4S_{3/2} \rightarrow {}^4I_{15/2}$ emission for σ excitation in the spectral range of the $^4I_{15/2} \rightarrow {}^4F_{5/2}$ transitions. The selected spectral ranges for the emission is indicated in Fig. 3 and the corresponding absorption transitions are indicated as in Fig. 4. The box indicates the fraction shown in an expanded scale in Fig. 6(a). The white straight lines are guidelines for the eye. For details see text.

in the window of our OMA so that they can be measured at one time. This approach yields the required high spectral reproducibility. Several ranges of peaks can be seen that correspond to the expected 3×5 transitions. In each of them the various sites become apparent. Besides giving an overview of the spectral data, this graph gives an instant impression how the different transitions are influenced by the change in the crystal environment. While some emission positions are almost independent of the excited Er^{3+} site, others drastically change in different energetic directions. The straight white lines can be used as a guideline for the eye to see this behavior, which is most apparent for the emission lines at around 2.255 eV and 2.245 eV. The spectral range indicated by a box is shown expanded in Fig. 6(a), so that more details can be illustrated.

At least 11 clear peaks can be found in this range belonging unambiguously to optically different Er^{3+} centers characterized by a specific excitation and emission energy. The associated peaks are labeled by numbers $1, \ldots, 11$ ordered according to increasing excitation energy. This identification is very straightforward in the stoichiometric sample due to narrow spectral widths, which yield steep peaks in the contour plot. The situation is less favorable for the congruent sample, which was studied with CEES for comparison (Fig. 7). As a consequence of the broader spectral transitions, the peaks are much less pronounced, but still all the sites found in stoichiometric crystal can be assigned again. Even two more spectral peaks (labeled 12 and 13) can be found.

2. Two-step excitation

In order to elucidate the role of the Er^{3+} site on the upconversion process, CEES can be measured also for the two-step excitation $^4I_{15/2} \rightarrow {}^4I_{11/2} \rightarrow {}^4F_{7/2}$ [see Fig. 1(c)]. For that purpose we chose the same spectral range for emission as above and selected the excitation energy at around 1.27 eV (980 nm). Due to the large number of transitions in this range (5×6), which additionally can be increased by the role of the second step, the contour plot is very complicated. Moreover, it becomes immediately apparent that more sites appear with strongly different excitation and emission energies than the ''regular'' sites found so far.

In order to illustrate this we show a contour plot for part of the data[28] in an expanded view [Fig. 6(b)] and in comparison with the direct excitation [Fig. 6(a)]. Examining first the peaks for the regular sites $(1, \ldots, 11)$, one finds that certain ones (e.g., site 3) almost vanish in the two-step excitation

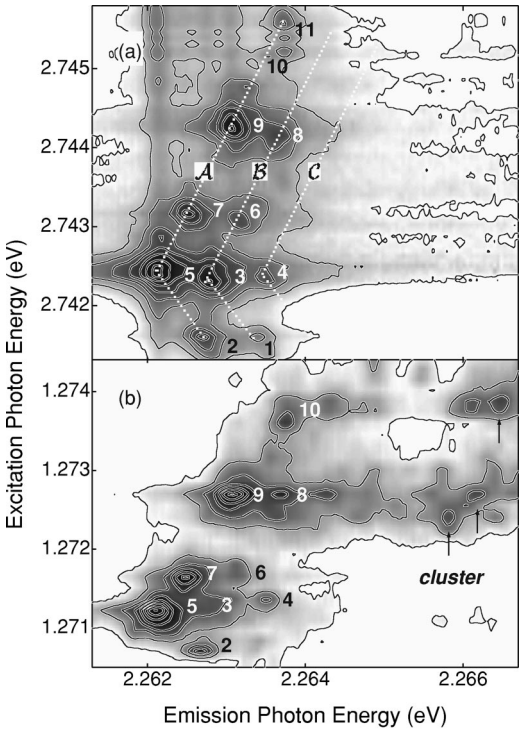

FIG. 6. Detailed CEES spectra for a stoichiometric sample in the range of the green $^4S_{3/2} \rightarrow {}^4I_{15/2}$ emission line with highest energy for (a) direct σ excitation in a $^4F_{5/2}$ level, (b) for two-step excitation σ excitation with 980-nm light via the $^4I_{11/2}$ level. The depicted spectral ranges are indicated in Fig. 5 by a box. The identified sites are labeled by numbers. The white dashed lines reflect the grouping into $\mathcal{A}$, $\mathcal{B}$, $\mathcal{C}$. For details, see text.

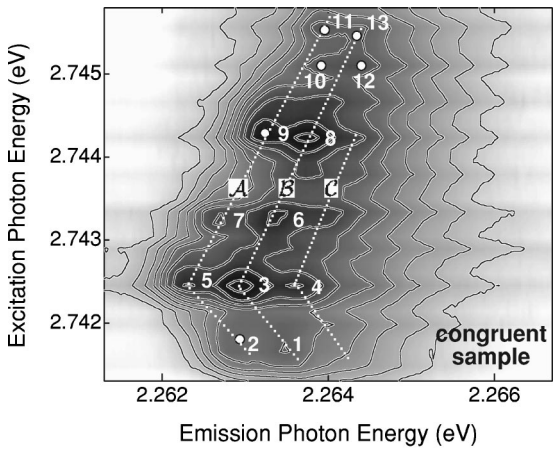

FIG. 7. Detailed CEES spectra for a *congruent* sample in the range of the green ${}^4S_{3/2} \rightarrow {}^4I_{15/2}$ emission line with highest energy for direct σ excitation in a ${}^4F_{5/2}$ level. The spectral range and the labeling are identical to Fig. 6(a).

case, while others become more pronounced (e.g., site 8). In other spectral regions this behavior can be reversed. For the chosen spectral range the additional peaks can be easily identified. They are characterized by a higher emission energy. Similar features have also been observed by Gill *et al.*[16] and they have been assigned to Er^{3+} clusters. We will adapt this notation here and give further arguments for this identification in the following discussion section. In the direct excitation these sites can only be found in careful measurements for excitation energies where the regular sites are absent (i.e., $E \geqslant 2.745$ eV). Even under these most favorable conditions the corresponding emission is at least 100 times weaker compared to the regular sites, suggesting that the clusters are very rare.

After the sites have been characterized in terms of their emission peak we can extract the *site-selective* upconversion excitation spectra out of the measured 2D data set that includes the complete spectral information. These spectra are shown for the two strongest well distinguished sites (5, 9) as well as for one of the cluster sites in Fig. 8. In order to take the relative abundances of the sites into account, we scaled the emission intensities for the two-step excitation with those measured for the respective site in the direct excitation. By doing so the spectra directly give a measure for the relative upconversion efficiency. In the comparison of these excitation spectra with the absorption spectrum we find good coincidences at several spectral positions and can thereby relate absorption peaks to the respective Er^{3+} center type. On the other hand, the excitation spectra deviate at some positions notably from the ground-state absorption most apparent on the high-energy side of the spectrum for site 9 for which we find features energetically higher than any expected ${}^4I_{11/2}$ absorption. Moreover, for sites 5 and 9, the relative height of the peaks notably differ from the absorption. These latter observations reflect the importance of the second step in the upconversion process. Due to the low abundance no absorption peak could be assigned to the clusters. The relative emission intensities for the different transitions, however, coincide well with the absorption spectrum of the regular sites. Comparing the strength of the upconverted emission among the different sites, we see that the cluster sites are much more

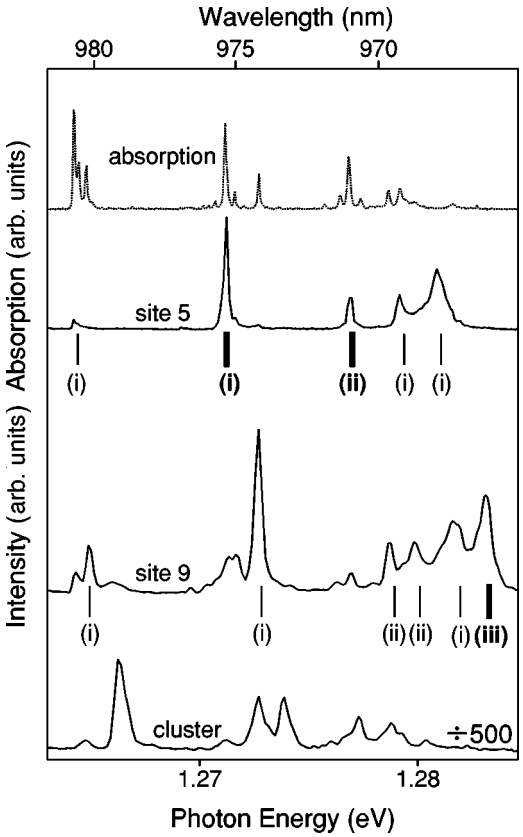

FIG. 8. Excitation spectra for two-step excitation via the ${}^4I_{11/2}$ level for three different emission energies representing the Er^{3+} sites 5 and 9 and some Er^{3+} clusters. The spectra are scaled with the emission intensity for the respective site in direct excitation. The ${}^4I_{15/2} \rightarrow {}^4I_{11/2}$ absorption spectrum is shown for comparison as a dashed line. The types of upconversion processes responsible for the respective peaks are indicated (compare Fig. 11). For details, see text.

efficient in their upconversion ($\times 500$), and even for the regular sites clear differences are found. Reasons and the underlying processes will be discussed below.

IV. EVALUATION AND DISCUSSION

Referring to the questions raised in Sec. I the experimental results presented here allow quite easily some initial statements:

(1) At least 11 regular sites exist. Additionally, one finds some very rare sites that participate preferentially in the upconversion process and are most likely related to small Er^{3+} clusters (i.e., two Er^{3+} on neighboring lattice sites).

(2) The spectral widths and the site distribution are different in the stoichiometric and congruent samples.

(3) The upconversion process depends strongly on the excitation energy and the participating Er^{3+} sites.

In the following we will discuss these aspects in more depth.

A. Identification of sites

From the detailed CEES spectrum in Fig. 6(a) the different sites can immediately be identified, yielding characteristic emission and excitation energies for the involved two

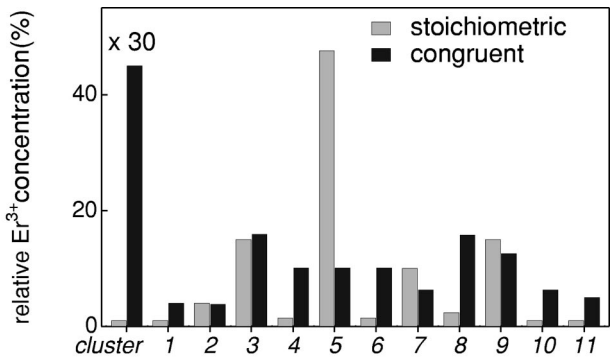

FIG. 9. Relative concentration of Er^{3+} ions on certain sites in stoichiometric and congruent samples.

transitions. The energy of other levels can then be determined successively by finding in the overview pictures (e.g., Fig. 5) other emission peaks for the same excitation or emission energy. In this way we can determine site selectively the crystal-field-split energy levels for the $^4I_{15/2}$, $^4I_{11/2}$, $^4S_{3/2}$, and $^4F_{5/2}$ states. A similar set of measurements for the red spectral region (not presented here) yields the energy levels for the $^4F_{9/2}$ state. The relative abundances of the sites can be obtained from the integrated emission intensities if (the almost constant) luminescence lifetimes are taken into account. All these results are summarized in Fig. 9 and Table I, representing a fingerprint of the Er^{3+} sites by which they can be identified even under variation of experimental conditions. For instance, we can correlate our site assignment with those used in other studies (see Table II). As one can see, mainly the strongest sites (3, 5, 8, 9) for the corresponding sample types have been reported in these earlier less detailed studies. In the attempt to order the sites by their energy levels (as is done by labeling the sites 1, . . . ,11 according to increasing energy for the highest $^4F_{5/2}$ level) it becomes apparent that no consistent scheme can be found, because the transition energies of one site compared to another are bigger in one spectral region and smaller in another. Most notably this is the case for the third and fourth levels of the ground state, which are almost degenerate for some (e.g., site 5) and shifted apart in opposite directions for others (e.g., site 9). Obviously the energy levels react quite differently to changes of the crystal-field environment.

On the question of the microscopic nature of the different local Er^{3+} environments, several studies exist with somewhat contradictory assumptions and models. Since our spectroscopic investigations are not sensitive to the chemical nature of the Er^{3+} neighbors, we adapt the results (obtained for the congruent material) from the ligand sensitive techniques (e.g., XSW), which determined that at least 90% of the Er^{3+} ions are located on or in the close vicinity of a Li^+ site (as shown in Fig. 10). The very broad distribution of the relative concentration of the different sites that we found for congruent samples (Fig. 9) therefore excludes the hypothesis that any major site is due to Er^{3+} on Nb^{5+} sites, as was speculated by Gill *et al.*[19] Our measurements also contradict the

TABLE I. Level energies (in eV) for several sites identified in the CEES spectra. Only those levels that could clearly be assigned are listed. A, . . . ,M label the corresponding absorption peaks.

	Site	1	2	3	4	5	6	7	8	9	10	11	cluster
$^4F_{5/2}$	M	2.7416	2.7416	2.7423	2.7423	2.7424	2.7430	2.7432	2.7441	2.7443	2.7452	2.7456	2.7453
	L	2.7352	2.7348	2.7351	2.7356	2.7346	2.7356	2.7352	2.7367	2.7362	2.7371	2.7370	2.7386
	K	2.7335	2.7329	2.7333	2.7338	2.7328	2.7338	2.7333	2.7344	2.7341	2.7347	2.7350	2.7369
$^4S_{3/2}$	G	2.2634	2.2627	2.2628	2.2635	2.2621	2.2632	2.2625	2.2636	2.2631	2.2638	2.2637	2.2662
$^4F_{9/2}$		-	-	1.9033	-	1.9027	-	-	-	1.9051	-	-	-
		-	-	1.9001	-	1.9008	-	1.9016	-	1.9024	-	-	-
		-	-	1.8900	-	1.8901	-	1.8906	-	1.8918	-	-	-
		-	-	-	-	-	-	-	-	-	-	-	-
		-	-	1.8782	-	1.8778	-	1.8781	-	1.8785	-	-	-
$^4I_{11/2}$	F	-	-	1.2810	-	1.2809	-	1.2818	-	1.2816	-	-	-
	E	-	1.2804	1.2794	-	1.2792	-	1.2798	-	1.2798	-	-	1.2773
	D	-	1.2757	1.2764	-	1.2769	-	1.2774	-	1.2787	-	-	1.2738
	C	1.2708	1.2707	1.2713	1.2713	1.2712	1.2717	1.2716	1.2727	1.2727	1.2736	-	1.2727
	B	-	-	-	-	-	-	-	-	-	-	-	-
	A	-	-	1.2644	-	1.2642	-	-	-	1.2649	-	-	1.2662
$^4I_{15/2}$		-	-	-	-	0.0498	-	-	-	0.0525	-	-	0.0529
		-	-	-	-	0.0455	-	-	-	0.0483	-	-	0.0492
		-	-	-	-	0.0419	-	-	-	0.0444	-	-	0.0456
		0.0226	0.0219	0.0219	0.0224	0.0213	0.0223	0.0216	0.0232	0.0226	0.0245	0.0230	0.0252
		0.0169	0.0160	0.0166	0.0177	0.0164	0.0177	0.0173	0.0201	0.0195	0.0200	0.0203	0.0197
		0.0159	0.0151	0.0155	0.0157	0.0156	0.0150	0.0154	0.0149	0.0153	0.0149	0.0163	0.0178
		0.0064	0.0064	0.0068	0.0068	0.0068	0.0070	0.0070	0.0076	0.0076	0.0080	0.0082	0.0084
		0	0	0	0	0	0	0	0	0	0	0	0

TABLE II. Labeling of sites in other publications in comparison with the present work.

Reference	Sample type	Name of site in Ref.	Name of site in this work
18	congr.	1,2	3,8
17	congr. fiber	two sites	3(+7?), 8
38	congr.	A,B	8,3
19	congr. + stoich.	1,2,3,4,5,6	5,3,9,8, cluster, cluster

distribution assumed for fitting recent EPR results[14] on identical samples, suggesting that some of the sites that we found are magnetically not easily distinguishable.

The Er^{3+} enters the $LiNbO_3$ in its trivalent state into a Li^+ site and therefore a charge-compensation is necessary that could be provided, for instance, by neighboring Li^+ vacancies. This local compensation persists even for stoichiometric samples that underwent the ''vacancy removing'' VTE procedure because we found well-defined sites that represent different types of local charge compensation. A delocalized compensation, as found for some Cr^{3+} sites,[30] can be excluded because it would lead to an inhomogeneous broadening of the spectral lines rather than to well-defined discrete transitions. Different from congruent $LiNbO_3$, the sharp lines in stoichiometric samples indicate that the more distant environment is very ordered. Based on these arguments we favor the picture that the Er^{3+} ion and the associated charge compensation form a defect complex that can extend over more than one unit cell and that is incorporated either into an highly ordered (stoichiometric) or quite disordered (congruent) $LiNbO_3$ crystal. This situation will result in narrow discretely distinguishable, site-specific, homogeneously broadened spectral lines in the first case and in inhomogeneously broadened lines in the latter case.

Within this picture the observed spectral shifts can be accounted for by a change in the internal electric field that the Er^{3+} experiences.[31] On the basis of an electrostatic approximation the extra fields caused by charge compensation (e.g., vacant Li^+ sites) and the associated effective negative charge on sites ($1^{\pm}$, $2^{\pm}$, $3^{\pm}$, or $4^{\pm}$ in Fig. 10) can be estimated to be in the order of 10^6 V/cm. The shifts of the crystal-field-split energy level expected for such additional fields due to an *internal* linear Stark effect can be predicted from *external* Stark effect measurements[32] and are—just as the observed ones—a few meV. In this estimate we have only considered the charge compensation by a single vacancy, but two of them are necessary. If we take this into account the number of possible configurations gets easily above the ≈ 11 we observed. However, in most cases one vacancy will have the dominant effect and the second will only slightly modify the spectral lines. Following this idea we can divide the identified sites (as indicated in Figs. 6 and 7 by the white dashed lines) in group $\mathcal{A}$ consisting of sites 2, 5, 7, 9, 10, 11, group $\mathcal{B}$ with sites 1, 3, 6, 8, 12, 13, and group $\mathcal{C}$ with site 4 and further rare (not labeled) sites. While within each group two sites differ by the way the *primary* charge compensation is achieved, the groups themselves reflect differences in the *secondary* compensation. This grouping is apparent both for stoichiometric and congruent samples. It seems that mainly a redistribution from one group to another takes place. While in the congruent sample before the VTE treatment type $\mathcal{A}$ is dominant, type $\mathcal{B}$ is most abundant afterwards in the stoichiometric sample. This makes it reasonable to assume that the redistribution of the defect configurations during VTE treatment dominantly involves the secondary more distant charge compensation. In this microscopic picture the different polarization behavior of sites 5 and 9 can be accounted for by a charge-compensating vacancy situated along the *c* axis for the first site and perpendicular to it for the latter site.

In addition to the regular sites discussed so far several more with stronger spectral shifts are found. Their number is very small already in congruent material but decreases even more with VTE treatment (Fig. 9). Motivated by the observed, much more efficient upconversion process and in accordance with Gill *et al.*,[16] we connect them to Er^{3+} clusters. The simplest type of them, the pair with Er^{3+} situated on neighboring Li^+ and Nb^{5+} sites that would not require any charge compensation, might be the prime candidate in our samples that have a relatively low Er^{3+} doping. The proximity between the complex partners can explain both the strongly different spectral positions and as we will discuss below the high upconversion efficiency. For these pairs several arrangements are possible that can account for the large number of cluster sites found.

B. Upconversion processes

On the basis of the detailed center characterization and spectral data the upconversion processes can be better described.

1. Regular sites

From the microscopic model described above we can assume that the regular sites are well separated from each other

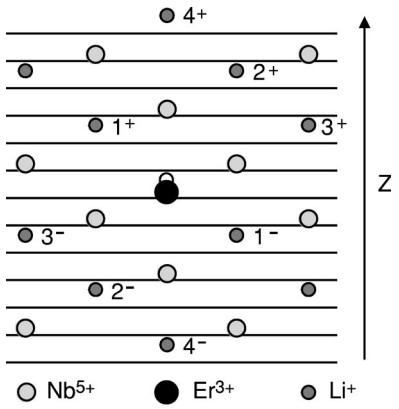

FIG. 10. Diagonal cut through the hexagonal unit cell of $LiNbO_3$ indicating the position of the Er^{3+} and of possible charge-compensating Li^+ vacancies labeled 1^+, 2^+, 3^+, 4^+, and 1^-, 2^-, 3^-, 4^- in $+c$ or $-c$ direction, respectively.

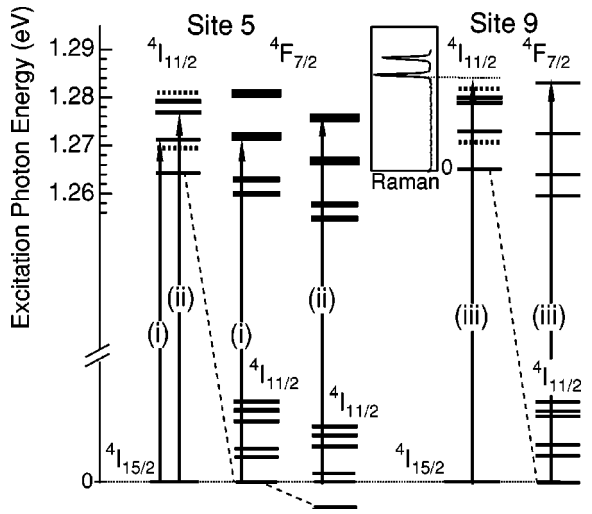

FIG. 11. Acurate energy level diagram for site 5 and 9. The $^4F_{7/2}$ levels are shifted by the indicated amounts to point out the matching energies and to illustrate three types of upconversion processes (i), (ii), and (iii). The levels for which σ or π transitions are expected for C_3 symmetry are drawn in solid and dotted lines, respectively. Aligned with its zero energy point to the lowest $^4I_{11/2}$ sublevel a Raman spectrum is depicted. For details, see text.

so that energy transfer processes can be excluded. In this case upconversion can only take place via successive absorption processes of photons with the same energies requiring accidental coincidence for the spectral positions of ground-state (GSA) and excited-state absorption (ESA). This condition is not easily and never perfectly fulfilled due to the sharp transition energies for our stoichiometric sample and the used narrow-band laser excitation. For that reason it is expected that not all GSA spectral positions can be seen and that the upconversion process cannot be observed for all sites. The multiplicity of Stark split levels, however, still offers various possibilities for the process to take place.

Three of these possibilities that we found to play a major role are schematically depicted in Fig. 11, where the involved energy levels are drawn for the main sites (5, 9). They are accurately deduced from the absorption data (Fig. 2). In order to emphasize the condition of coinciding GSA and ESA we shift the excited state $^4I_{11/2}$ from which ESA occurs down to zero energy. Drawing the levels that way, one sees that the upconversion process can only take place for those excitation energies for which two levels of the $^4I_{11/2}$ and $^4F_{7/2}$ coincide.

In the first process (i), based on a direct excited-state absorption, the Er^{3+} ion relaxes after the first excitation step into the lowest $^4I_{11/2}$ state from which ESA can occur. The corresponding spectral position is marked with a thick line in the excitation spectrum in Fig. 8. Besides the explicitly depicted case this type of process is responsible for the majority of peaks (thin lines) in the excitation spectra. As shown in Fig. 1 and indicated as solid lines for the final state in Fig. 11, most of the GSA transitions are σ polarized and, hence, the observed upconversion process is most efficient for σ-polarized excitation light. Moreover, under these σ-excitation conditions even processes involving π-type GSA transitions are clearly visible, especially for the excitation energy of the highest $^4I_{11/2}$ sublevel for which an almost perfect overlap with the highest $^4F_{7/2}$ sublevel exists. This is due to the imperfect C_3 symmetry of the centers, but it may also reflect small misalignments of the sample.

In process (ii), which is based on thermal activation, the GSA is followed by a ESA out of higher $^4I_{11/2}$ sublevels. At $T=5$ K the relative population of the second lowest level is extremely small, making the process fairly unlikely. Only due to the otherwise almost perfect spectral overlap of GSA and ESA does this process become observable as depicted (Fig. 11) for the excitation energy marked in Fig. 8 by a thick line. However, because of its inherent strong temperature dependence it will become a preferred upconversion channel at higher temperatures.

In process (iii), a phonon-assisted process, the crucial role of the coupling to the crystal lattice becomes apparent. In this case no zero-phonon GSA transition is in resonance with the excitation photon. However, the energy difference between the excitation energy and the energy of the strong GSA transition to the lowest excited state corresponds exactly to a phonon as indicated by the depicted piece of a Raman spectrum. Under these conditions a phonon-assisted GSA is followed by a well-matched ESA out of the lowest $^4I_{11/2}$ sublevel. This process could be found in a pronounced form only for site 9. While this is the only case in which the excitation spectrum of the upconverted luminescence does not coincide with the GSA spectrum for the 980-nm region, this situation has been encountered more frequently in other spectral excitation regions[18] (800 nm, 650 nm) and is sometimes accompanied by a photon avalanche process.[33,34,15]

The excitation position at which these different processes take place for the different main regular center types (5, 9) are indicated in Fig. 8. It becomes obvious that the kind of process involved in the upconversion strongly depends on the excitation wavelength and Er^{3+} site. For all described processes we can convince ourselves that at lowest temperatures the conditions are not optimal in terms of high upconversion efficiency for the stoichiometric sample. Broadening the optical transitions by increased temperature or in less perfect crystalline environments as found in congruent bulk $LiNbO_3$ crystals and waveguides makes upconversion processes—as we observed—more likely.[35]

2. Cluster sites

The much higher upconversion efficiency of certain sites suggests that a different process is involved for them. The main candidate and the reason why we assumed that these sites are clusters is an energy transfer process among closely neighboring Er^{3+} ions. For the electric dipole-dipole interaction between the two ions the Förster-Dexter type energy transfer rate W_{DA}^{dd} can be estimated by the following relation:[36]

$$W_{DA}^{dd}=\left(\frac{1}{4\pi\epsilon_o}\right)^2\frac{3\pi\hbar e^4}{n^4m^2\omega^2}\frac{1}{R^6}f_Df_A\int g_Dg_AdE,$$

with f_D, f_A, and g_D, g_A as the oscillator strength and the normalized form function of the transition of the donor and acceptor ion, respectively. For energy transfer from an excited Er^{3+} (D^*) and to the neighbor (A), which is in the ground state, we find the rate $W_{D^*A}^{dd}\approx 7\times 10^6$ s^{-1} by taking

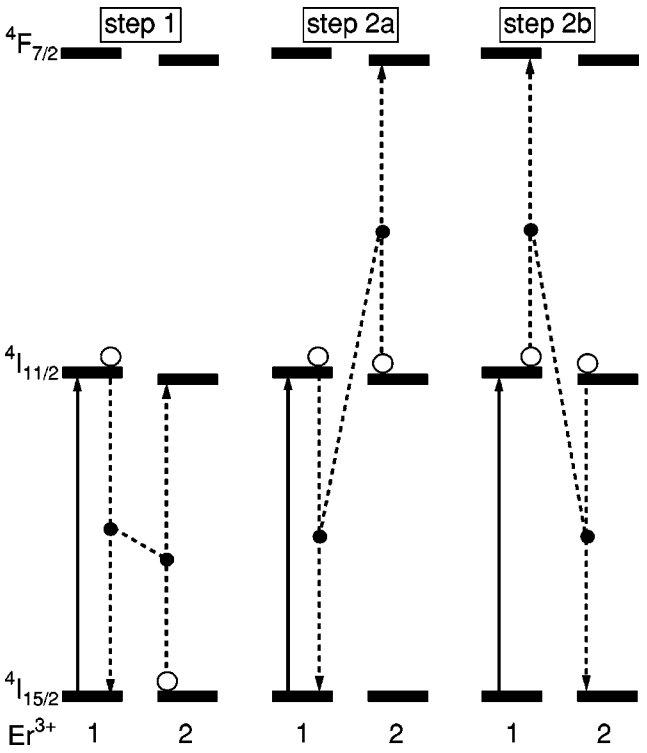

FIG. 12. Simplified energy level diagrams illustrating the upconversion processes within clusters. Solid arrows indicate optical excitation, and the dotted lines represent the energy transfer processes. For details, see text.

the constants ($\epsilon_o, m, e\hbar$) with their usual meaning, n for the refractive index of $LiNbO_3$, $f_{D^*}=f_A=120\times10^{-8}$ (Refs. 37 and 38) for the $^4I_{15/2}\leftrightarrow{}^4I_{11/2}$ transition, and $R\approx4\times10^{-10}$ m as the distance between an Er^{3+} on Li^+ site and one on a Nb^{5+} site and if we assume perfect spectral overlap of the Lorentzian line profiles (FWHM = 0.1 meV). This rate is easily able to compete with the other partially nonradiative transition processes ($W\approx5\times10^3$ s^{-1}) for the $^4I_{11/2}$ level even if the overlap is not perfect and phonons have to make up for the energy mismatch. Similarly, the transfer rate between two excited ions (D^*,A^*), which leads to deexcitation (cross relaxation) of the one and further excitation of the other, can be estimated to be $W^{dd}_{D^*A^*}\approx10\times10^6$ s^{-1} using $f_{A^*}=180\times10^{-8}$ (Ref. 29) for the oscillator strength of the $^4I_{11/2}\rightarrow{}^4F_{7/2}$ transition. In order to lead to an energy upconversion within a defect pair two photons need to be absorbed, and the described two energy transfer processes have to take place successively. In the following we will discuss how this can occur most efficiently (see Fig. 12). We continue to consider only the most favorable case of a Er^{3+} defect pair located on neighboring Li^+ and Nb^{5+} sites. The two Er^{3+} ions certainly experience a different crystal field and hence they will differ in their transition energies. For that reason the pump-photon energy can only be in resonance with the $^4I_{15/2}\rightarrow{}^4I_{11/2}$ transition of one of the two Er^{3+} ions.

In a first step this Er^{3+} ion will be optically excited and relax into the lowest excited $^4I_{11/2}$ sublevel from where it will quickly transfer the energy to its neighbor. At low temperature this process will preferentially go towards lower energies and therefore we have to assume that the first Er^{3+} has higher transition energies than the second, as indicated in Fig. 12. The observation that the upconverted green luminescence is excited in general at higher energies for cluster sites compared to the regular ones might be a direct consequence of that condition.

In the second step, renewed excitation of the first Er^{3+} within the $^4I_{11/2}$ lifetime leads to a situation where both partners are excited. They can exchange their energy via a cross-relaxation process, which brings one of the ions into the $^4F_{7/2}$ and the other back to the ground state. Which one of the two will end up in the excited state depends on details of the energy levels. The two possible processes (step 2a or 2b) are shown in Fig. 12. Although a final decision cannot be made we favor step 2b based on our results. It leads to excitation of the Er^{3+} ion, which has its energy levels at higher energies explaining the higher energies of the observed upconverted green luminescence of the cluster in comparison to the regular sites.

Independent of this last question, the upconversion process based on energy transfer can be much more efficient than the ESA process because the incident photon has to obey just one resonance condition for the GSA and not two (ESA, GSA) as was necessary for the regular sites. By changing the excitation energy this condition can be fulfilled and therefore the excitation spectrum for the upconverted luminescence resembles, as can be seen in Fig. 8, quite closely the absorption of one of the ions within the cluster.

V. SUMMARY AND CONCLUSIONS

We found by high-resolution CEES a large number of Er^{3+} sites and characterized them with respect to their abundance, energy levels, and redistribution by the VTE treatment. Several different upconversion processes could be identified that depend both on site and on the excitation energy. Although some new information about the microscopic Er^{3+} center configuration could be obtained a complete picture awaits results from further site-sensitive techniques that preferentially should be applied in combination with the optical spectroscopy studies. Several attempts in that direction, e.g., magnetic resonance, hydrostatic pressure, and Stark effect, are currently under way, with promising first results.[39]

In view of the development of the potential upconversion-based laser the site distribution found is unfavorable because for a given excitation energy only a certain ensemble of ions will be able to participate. For that reason, it would be desirable to be able to control the site distribution. As we have demonstrated, the VTE treatment can be considered as a step in this direction. Concentration variation, codoping, and systematic tempering experiments could be others.

ACKNOWLEDGMENTS

This work was performed as a project within the DFG funded Forschergruppe (research group) ''Integrierte Optik in $LiNbO_3$'' in the laboratory of Professor W. von der Osten. The authors gratefully acknowledge numerous important discussions on the topics with Professor A.A. Kaplyanskii, Dr. A.B. Kutsenko, and Professor W. von der Osten. We are also very thankful to Professor S. Kapphan and his group for performing the VTE treatments.

[1] I. Baumann, S. Busso, R. Brinkmann, R. Corsin, M. Dinand, A. Greiner, K. Schäfer, J. Söchtig, W. Sohler, H. Suche, and R. Wessel, IEEE J. Sel. Top. Quantum Electron. **2**, 355 (1997).
[2] R. M. Macfarlane, E. A. Whitacker, and W. Lenth, Electron. Lett. **28**, 2136 (1992).
[3] R. Brede, E. Heumann, J. Koetke, T. Danger, and G. Huber, Appl. Phys. Lett. **63**, 2030 (1993).
[4] F. Heine, E. Heumann, T. Danger, T. Schweizer, and G. Huber, Appl. Phys. Lett. **65**, 383 (1994).
[5] S. A. Pollack, D. B. Chang, M. Birnbaum, and M. Kohta, Proc. SPIE **1410**, 156 (1991).
[6] H. Yanagita, I. Masuda, T. Yamashita, and H. Toratani, Electron. Lett. **26**, 1836 (1990).
[7] V. Lupei, S. Georgescu, and V. Florea, IEEE J. Quantum Electron. **29**, 426 (1993).
[8] T. Gog, M. Griebenow, and G. Materlik, Phys. Lett. A **181**, 417 (1993).
[9] T. Gog, M. Griebenow, T. Harasimowicz, and G. Materlik, Ferroelectrics **153**, 249 (1994).
[10] L. Kovács, L. Rebouta, J. C. Soares, and M. F. da Silva, Radiat. Eff. Defects Solids **119-121**, 445 (1991).
[11] C. Zaldo and C. Prieto, Ferroelectrics **134**, 47 (1992).
[12] L. Rebouta, M. F. da Silva, J. C. Soares, D. Serrano, E. Diéguez, F. Agulló-López, and J. Tornero, Appl. Phys. Lett. **70**, 1070 (1997).
[13] I. Baumann, R. Brinkmann, M. Dinand, W. Sohler, L. Beckers, C. Buchal, M. Fleuster, H. Holzbrecher, H. Paulus, K.-H. Müller, T. Gog, G. Materlik, O. Witte, H. Stolz, and W. von der Osten, Appl. Phys. A: Mater. Sci. Process. **64**, 33 (1997).
[14] T. Nolte, T. Pawlik, and J.-M. Spaeth, Solid State Commun. **104**, 535 (1997).
[15] L. Nuñez, B. Herreros, R. Duchowicz, G. Lifante, J. O. Tocho, and F. Cussó, J. Lumin. **60&61**, 81 (1994).
[16] D. M. Gill, J. C. Wright, and L. McCaughan, Appl. Phys. Lett. **64**, 2483 (1994).
[17] W. Jia, K.-S. Lim, H. Liu, Y. Wang, J. J. Lu, S. I. Yun, F. E. Fernandez, and W. M. Yen, J. Lumin. **66&67**, 196 (1997).
[18] O. Witte, H. Stolz, and W. von der Osten, J. Phys. D **29**, 561 (1996).
[19] D. M. Gill, L. McCaughan, and J. C. Wright, Phys. Rev. B **53**, 2334 (1996).
[20] The crystals were grown in the group of K. Polgar at the Hungarian Academy of Science, Budapest.
[21] R. l. Holman, in *Processing of Crystalline Ceramics,* edited by H. Palmour, R. Davis, and T. M. Hare (Plenum, New York, 1978), p. 343.
[22] P. F. Bordui, R. G. Norwood, D. H. Jundt, and M. M. Fejer, J. Appl. Phys. **71**, 875 (1992).
[23] The VTE treatment was performed in the group of Professor Kapphan at the Universität Osnabrück.
[24] A. Ridah, P. Bourson, M. D. Fontana, and G. Malovichko, J. Phys.: Condens. Matter **9**, 9687 (1997).
[25] L. Kovács, V. Szalay, and R. Capelletti, Solid State Commun. **52**, 1029 (1984).
[26] L. Kovács, M. Wöhlecke, A. Jovanivić, K. Polgár, and S. Kapphan, J. Phys. Chem. Solids **52**, 797 (1991).
[27] W. M. Yen, W. C. Scott, and A. L. Schawlow, Phys. Rev. **136**, 271 (1964).
[28] The contour plot of the complete data set of this and other spectral ranges can be obtained directly from the authors.
[29] G. Malovichko, V. Grachev, E. Kokanyan, and O. Schirmer, Phys. Rev. B **59**, 9113 (1999).
[30] D. M. B. P. Milori, I. J. Moraes, A. C. Hernandes, R. R. de Sousa, M. Siu-Li, M. C. Terrile, and G. E. Barberis, Phys. Rev. B **51**, 3206 (1995).
[31] A. A. Kaplyanskii (private communication); (unpublished).
[32] K. Polgár and A. P. Skvortsov, Opt. Spectrosc. **58**, 140 (1985).
[33] F. Auzel and Y. Chen, J. Lumin. **65**, 45 (1995).
[34] M.-J. Joubert, Opt. Mater. **11**, 181 (1999).
[35] V. Dierolf, A. B. Kutsenko, and W. von der Osten, J. Lumin. **83-84**, 487 (1999).
[36] B. Henderson and G. F. Imbusch, *Optical Spectroscopy of Inorganic Solids, Monographs on the Physics and Chemistry of Materials* (Clarendon Press, Oxford, 1989).
[37] V. Dierolf, A. B. Kutsenko, C. Sandmann, F. Tallian, and W. von der Osten, Appl. Phys. B: Lasers Opt. **68**, 767 (1999).
[38] J. Amin, B. Dussadier, T. Schweizer, and M. Hempstead, J. Lumin. **69**, 17 (1996).
[39] V. Dierolf, A. B. Kutsenko, C. Sandmann, Th. Tröster, and G. Corradi, J. Lumin. (in press).